



A Comparison of Different Approaches for Predicting Transonic Buffet Onset on Infinite Swept Wings

Kirill V. Belyaev¹ , Andrey V. Garbaruk¹ , Sergey V. Kravchenko² ,
Michael K. Strelets¹ 

© The Authors 2022. This paper is published with open access at SuperFri.org

A comparative study is performed on three different approaches for prediction of transonic buffet onset on infinite swept wings. All three approaches are based on the unsteady Reynolds-averaged Navier–Stokes (URANS) equations, and include: quasi-3D and fully-3D global stability analysis of the corresponding steady 2.5D RANS solutions and direct numerical solution of the 3D URANS equations. The results are presented for an infinite swept wing based on the ONERA OAT15A airfoil section. The quasi-3D stability analysis is shown to be accurate and most efficient and, thus, is best suited for this spanwise-uniform flow. The fully-3D stability analysis ensures the same accuracy, provided that the grid-step in the spanwise direction is sufficiently small. It is much more demanding in terms of computer memory but can be extended to more-general wing configurations. Good agreement is observed between the three approaches in terms of critical conditions for buffet onset and the instability growth characteristics, providing a cross-validation of the methods and an assessment of their computational demands.

Keywords: transonic buffet onset, infinite swept wing, global stability analysis, quasi-3D and fully-3D approaches, direct URANS solution.

Introduction

Transonic buffet phenomenon is characterized by self-sustained oscillations of the shockwave that forms on the upper surface of airplane wings. At Mach numbers typical of cruise flight for commercial airliners ($M = 0.75 - 0.9$), these shock oscillations turn out to be rather intensive over a wide range of angles of attack and lead to large airplane-level normal accelerations. This can limit the maximum allowable angle of attack, and, therefore, the maximum lift and also the flight altitude. Hence, a determination of the conditions for the buffet onset and its characteristics is essential for airplane design, and it is not surprising that different aspects of this phenomenon (its mechanism, critical values of the onset Mach number and angle of attack, and post-onset unsteady characteristics) have been investigated in a very large number of experimental and numerical studies (see the review of Giannelis et al. [6], and more recent papers [2, 3, 8, 12–17, 21, 23]).

According to the experimental studies, the shock-wave oscillations observed in transonic-wing flow after buffet onset are characterized by frequencies that are much smaller than the frequencies associated with turbulent fluctuations typical of high-Reynolds-number aerodynamic flows. This justifies modeling of the buffeting flows and predicting the buffet onset based on the direct time-accurate numerical integration of the unsteady Reynolds-averaged Navier–Stokes equations (URANS). Along with this, it is now generally accepted that the buffet phenomenon is explained by the onset of a global instability in transonic-wing flows at supercritical values of the Mach number and angle of attack [6]. This opens the possibility of using an alternative approach to predicting the buffet onset, namely, applying global stability analysis to steady RANS solutions. The applicability of this approach was first demonstrated for two-dimensional

¹Peter the Great Saint-Petersburg Polytechnic University, Saint-Petersburg, Russian Federation

²The Boeing Company, Chicago, USA

(2D) airfoil buffet [1, 4], and the approach is now widely used in the investigation of buffeting flows (see, e.g. [2, 3, 14, 15, 23]).

Extensions of the approach to quasi-three-dimensional (q-3D) flows for application to infinite swept wings have been presented in the works [2, 14, 15]. Meanwhile, fully-three-dimensional (3D) stability analysis has been used to analyze a swept tapered wing [23]. More recently, He and Timme [8] used the fully-3D approach to analyze an infinite swept wing. This shows the linkage between the discrete modes of the fully-3D analysis and the continuous band of modes predicted by the q-3D analysis. The work of He and Timme [8] also considered the effects of a stationary mode as part of the baseflow for the onset of oscillations on an unswept wing. This is possible with the fully-3D analysis, but not the q-3D approach.

Here, we provide a quantitative comparison between the q-3D and fully-3D stability approaches for the infinite swept wing, along with comparisons to the unsteady simulations. These three approaches involve independent formulations, but all flow variables and turbulence-model parameters are matched for the comparisons, allowing an assessment of both the accuracy and the efficiency for varying spanwise representations.

In this article, the comparisons are carried out for an infinite swept wing based on the ONERA OAT15A airfoil section [10]. First, in Section 1, we briefly present an overview of the three approaches. Then, in Section 2, we discuss the basic flow conditions and some of the numerical aspects of the performed computations. In Section 3, results are presented and discussed. Finally, in Conclusion, we summarize the major findings of the study.

1. Overview of the Considered Approaches

Steady flows past an infinite swept wing are characterized by uniformity in the spanwise directions z , with flow variation dependent only on x and y (see Fig. 1). Hence, such flows may be computed by numerical integration of the RANS equations in which the spanwise derivatives are set zero, that is, within an effectively 2D problem statement. In order to distinguish this type of flow from the purely-2D and fully-3D flows it is often referred to as 2.5D flow (with flow in the z direction, but $\partial/\partial z = 0$).

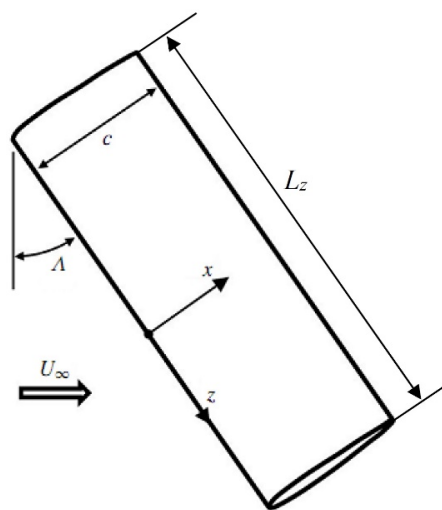


Figure 1. Schematic of section of infinite swept wing with the length L_z

The critical values of the angle of attack and Mach number corresponding to transonic buffet onset in the 2.5D flows may be determined using any of the three approaches based

on the RANS equations. The first approach involves the direct numerical integration of the full 3D URANS equations for a wing section with a span length L_z (a free parameter of the problem) using periodic boundary conditions in the z -direction and a steady solution of the 2.5D RANS equations as initial conditions. For subcritical values of the angle of attack, $\alpha < \alpha_{crit}$, corresponding to a given Mach number, the URANS solution does not change in time, whereas for supercritical values $\alpha > \alpha_{crit}$, the solution is characterized by exponential growth of flow disturbances (deviations from the initial conditions). Thus, a series of 3D URANS computations at different values of α and L_z provides the critical buffet-onset conditions and the corresponding post-critical growth rate and frequency of the disturbances, based on post-processing of the simulation time-histories in the linear stage of the solution. The spanwise domain length L_z selects the admissible spanwise wavelengths for the disturbance, so multiple values should be considered. Along with this, based on the developed non-linear stage of the solution, one can compute the unsteady and mean local and integral aerodynamic characteristics of the buffeting flow, e.g. the lift and drag of the wing. This approach is the most general, but it demands large computational resources needed for performing multiple 3D unsteady simulations. Additionally, when close to critical buffet-onset conditions where disturbances grow or decay very slowly with time, the simulations require extremely long time samples and results can be highly sensitive to numerics.

Two alternative approaches for investigating buffet-onset conditions are based on global stability analysis of the 2.5D steady RANS solutions at different angles of attack. These approaches employ linear stability equations for describing the disturbances, which are derived by decomposing the total flow field into a steady baseflow and a small superimposed perturbation. Note that in the presence of shock waves, this is, strictly speaking, impossible, but still seems to be justified for the numerical solutions, if the perturbations are sufficiently small not to change the set of the grid cells “occupied” by the shock (i.e., if the shock remains effectively still). After introducing the decomposition into the 3D URANS equations with associated boundary conditions, and canceling terms which describe the steady RANS solution, the equations are linearized to provide a system of equations for the small 3D disturbances. Nontrivial solutions to this system are found by solving an eigenvalue problem for the corresponding linear differential operator [4]. The real and imaginary parts of the complex eigenvalues represent the frequency and the growth/decay rate (depending of the sign), respectively. The associated eigenfunction provides the spatial distribution for the disturbance. Hence, in order to answer the question on whether the considered steady solution is stable or unstable in the framework of these approaches, it is sufficient to find the eigenvalue with the maximum growth rate. If this value turns out to be negative, the steady solution is stable and otherwise it is unstable.

The first of the stability approaches, the q-3D approach, uses the spanwise invariance of the steady baseflow, and decomposes the disturbance into Fourier modes in z . Each mode is characterized by a spanwise wavelength λ_z , defined by the wave number β ($\lambda_z/c = 2\pi/|\beta|$), which is a free parameter of the q-3D stability problem. As a result of the Fourier decomposition in z , the q-3D eigenmodes are two-dimensional and sometimes referred to as “biglobal” [22]. The computational cost for this approach (both in CPU time and, especially the computer memory) is much less than for the URANS simulations or the fully-3D stability analysis described below. Not surprisingly, this method is widely used in the literature (see, e.g. [2, 3, 14]). However, for problems in which the steady baseflow is not strictly uniform in the spanwise direction, the q-3D formulation is only an approximation.

Thus, a more-general form of the stability problem is given by the fully-3D approach. Rather than introducing a Fourier decomposition in z , this approach considers a 3D eigenmode extending over the spanwise domain L_z . This is sometimes referred to as “triglobal” stability analysis [22]. In this formulation, the spanwise wavelength is set by the domain size L_z , just as it is in the URANS simulations. Note that in principle (neglecting any difference in the discretization errors of the URANS equations and the equations for the disturbances), predictions of the critical values for buffet onset based on the fully-3D stability analysis should coincide with those predicted based on the 3D URANS simulations, provided that the latter are started from the baseflow with superimposed disturbances of a very small amplitude (see below). However, computational resources needed for implementation of these two approaches are quite different: the 3D stability analysis is much less expensive than 3D URANS in terms of the CPU time, but is much more demanding in terms of computer memory, which strongly limits the size of the computational grids. For the current analysis of a 2.5D baseflow, this fully-3D analysis can be directly compared to the q-3D analysis, allowing an independent validation of each approach.

2. Flow Regimes and Numerical Aspects of Computations

Specific computations performed in the present work are carried out for an infinite-span wing based on the supercritical airfoil OAT15A at different angles of attack α varying in the range from 2.75° up to 3° and fixed values of the wing sweep angle $\Lambda = 30^\circ$, Reynolds number $Re_n = U_n c / \nu = 3 \cdot 10^6$ and Mach number $M_n = U_n / a_\infty = 0.73$. Nondimensionalization is based on the normal to the wing leading edge component of the free-stream velocity $U_n = U_\infty \cos \Lambda$. The boundary-layer flow is assumed to be fully turbulent and is modeled using the Spalart–Allmaras turbulence model [19] with the Compressibility Correction [20] (SA CC model), which has been successfully used in many transonic buffeting flows (see, e.g. [1–4, 14]).

Computations are carried out with the in-house computer codes developed by the authors. In particular, the compressible steady and unsteady RANS equations are solved using the code of Numerical Turbulence Simulation (NTS) [18], and the algorithms implemented for solutions of the stability problems are presented in detail in [1, 2, 4]. The NTS code accepts structured multi-block overset grids. Computational domain and grid are divided into a set of grid blocks, taking into consideration both the flow geometry and effective usage of computers with large amount of nodes/cores. For massively parallel computations, the code employs a so-called hybrid Message Passing Interface (MPI)/Open Multi Processing (Open MP) parallelization scheme, which ensures a high efficiency of simulations on very large computational grids required for 3D URANS and scale-resolving simulations (see, e/g. [7]). Within this approach, both MPI libraries (with distributed memory technologies) and Open MP libraries (with shared memory technologies) are used for parallelization of computations in different grid blocks (or set of grid blocks). This strategy is very flexible and is easy to adapt to computers with different architecture by manually varying a set of managing parameters. The code has been thoroughly validated by comparisons with the solutions of a wide range of aerodynamic and stability problems and experimental data available in the literature.

The computational domain and the grid in the XY-plane used for the computations are shown in Fig. 2. The domain has a radius of about $30c$, which, along with the use of the characteristic non-reflecting boundary conditions with the Riemann invariants computed by the free-stream flow parameters, ensures an adequate representation of the transonic flow past the wing. The structured computational grid has two overlapping blocks, shown in Fig. 2 by blue

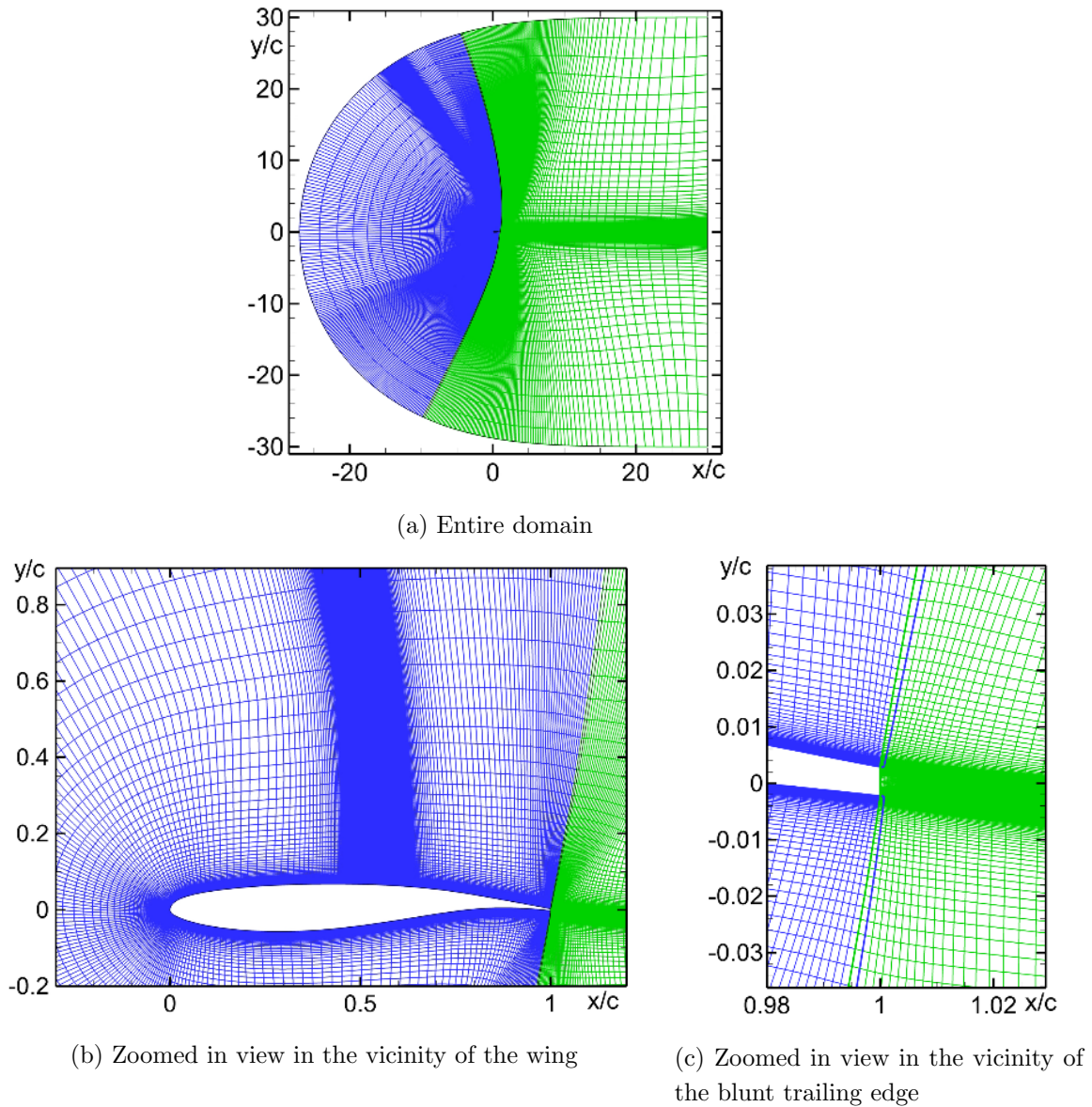


Figure 2. Computational domain and two-block grid in XY plane

and green grid lines. The main (blue) block is a C-grid with 343×140 cells, and the second (green) block is an H-grid with 97×374 cells. As a result, the total cell count of the grid in the XY-plane is about 85,000. In the streamwise direction the grid-step was reduced by a factor of ten over a wide area encompassing the shock location (in this area $\Delta x/c \approx 0.002$). The step in the wall-normal direction was decreased toward the wing surface so that the size of the first near-wall cell in the coordinates of the law of the wall $\Delta_{y,1}^+ = \Delta_{y,1} u_\tau / \nu$ ($u_\tau = \sqrt{\tau_w / \rho}$ is the friction velocity) is less than 1.0.

The span length of the computational domain L_z used in the 3D URANS (this size defines the maximum wavelength of the solution) was set equal to $2c$, and the grid spacing in the z -direction Δz is uniform and equal to $0.005c$, which ensures sufficient resolution (not less than 20 cells per wavelength) of disturbances with length $\lambda_z > 0.1c$ (as will be shown shortly, for all the considered flows the most unstable modes have wavelengths within this range). As a result, the number of spanwise grid planes is $N_z = 400$, and the total cell count for the 3D URANS-simulation grid is around 35 million.

Time-integration of the URANS equations in the NTS code is performed with the use of the implicit three-layer backward scheme of second-order accuracy with the time-step $\Delta t = 10^{-3} \cdot c/U_n$, which ensures the Courant-Friedrichs-Lewy criterion $CFL < 1.0$ everywhere except for the close vicinity of the wing surface with extremely small wall-normal steps Δy .

The flow-fields used to initialize the unsteady simulations are chosen based on the angle of attack. Particularly, for $\alpha \geq 2.9^\circ$ (i.e., well above the critical angle of attack for buffet onset, see Fig. 10 below), the simulations are initiated with steady RANS solutions. At the lower α values, the initial fields are obtained by superposing the corresponding steady solutions with eigenvectors from the stability analysis with small (10^{-6}) amplitude. For the simulation at $\alpha = 2.8^\circ$ (stable according to URANS), this is the only way to determine the negative growth-rate (decay rate) in the URANS framework. At $\alpha = 2.85^\circ$, close to the URANS critical value, this approach offers a huge savings in CPU time; using only the steady RANS initial field, the time sample $T = c/U_n$ needed for development of the instability and extraction of the growth-rate would be an order of magnitude larger.

In principle, the fully-3D stability analysis provides simultaneous results for disturbances to the steady RANS solutions with wavelengths $\lambda_z = L_z/m$, where m is an arbitrary natural number. However, as mentioned above, this approach demands very large computer memory and, hence, imposes severe restrictions on the size of the computational grid. Particularly, with the memory available for the computations performed in the present study, the maximum affordable grid size for the fully-3D stability analysis is about 2 million cells. With the XY grid of 85,000 cells, this allows a maximum number of cells in the spanwise direction of $N_z = 22$. Thus, for a single solution only the disturbances at the maximum wavelength $\lambda_z = L_z$ may be analyzed reliably (i.e., with greater than 20 cells per wavelength). In order to consider different wavelengths, instead of using one computation in the domain with $L_z/c = 2$, as in the 3D URANS simulations, a series of 3D stability analyses are carried out with a fixed number of $N_z = 22$ cells in the spanwise direction, but with L_z/c varying over the range 0.5 up to 25. This ensured that the stability analysis only considered well resolved disturbances, i.e., those having the maximum wavelength $\lambda_z = L_z$ or the wave number $\beta = 2\pi/L_z$.

Finally, the q-3D stability analysis is performed using the same XY grid as the URANS simulations and the fully-3D stability analysis. Calculations are conducted for different values of β (a free parameter within this approach), varying in the range from $2\pi/25$ up to $2\pi/0.5$, i.e., in the range corresponding to the wavelengths addressed in the fully-3D analysis.

3. Results and Discussion

In order to show the basic character of the instability for transonic flows past an infinite swept wing, we first present results from the q-3D stability analysis for the considered flow at $\alpha = 2.95^\circ$. An extensive discussion of this problem is available in earlier papers [2, 14]. Building on this example, the primary results are then presented for the direct comparison of predictions using the three different approaches: q-3D stability analysis, fully-3D stability analysis, and 3D URANS simulations.

3.1. Baseflow and Q-3D Stability Results

Figure 3 illustrates major features of the steady 2.5D RANS solutions used for the stability analysis. It shows contours of the Mach number in XY-plane and streamwise distributions of

the skin-friction and pressure coefficients C_f and C_p over the wing surface at $\alpha = 2.95^\circ$, as an example. One can see that the flow is characterized by the formation of a shock closing the supersonic region above the suction side of the wing. This shock induces separation of the boundary layer, which extends downstream to the wing trailing edge for this particular value of α .

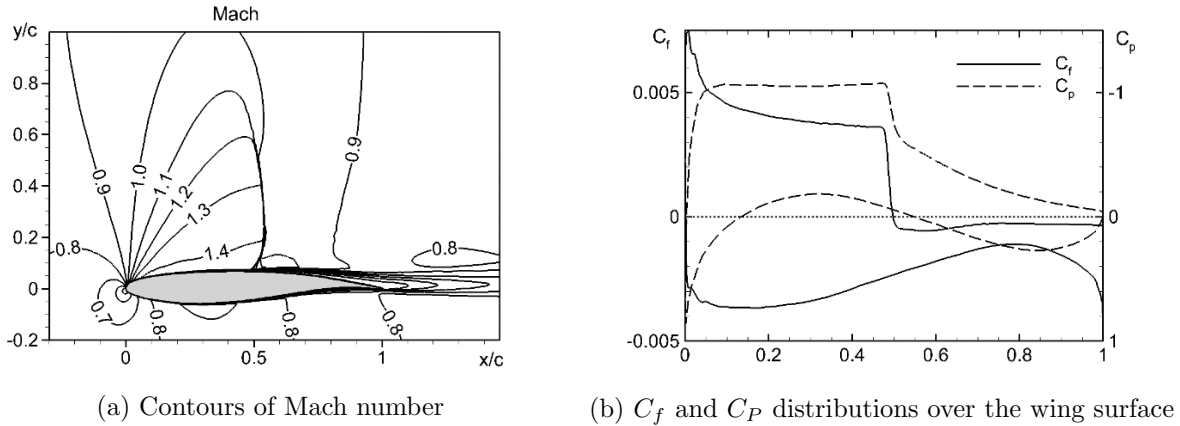


Figure 3. Steady 2.5D RANS solution (baseflow) for OAT15A swept wing at $\alpha = 2.95^\circ$, $M_n = 0.73$

As shown in [2, 14], for transonic flows past swept wings, the q-3D analysis predicts two modes of instability, an oscillatory mode and a traveling propagating outboard mode. There can be two characteristic wavelengths for the traveling modes ($\lambda_z \approx c$ and/or $\lambda_z \approx 0.1c$), depending on the values of M_n and α . Figure 4 illustrates the mode shapes for the u -component of the eigenvectors corresponding to the spanwise uniform ($\beta = 0$) oscillatory mode and the traveling mode at $\beta = 2\pi$ ($\lambda_z = c$). The Figure shows that the two modes are qualitatively similar. The oscillatory mode has maximums at the shock and in the separated shear layer, with the magnitude at the shock roughly 20 times larger than in the shear layer. In contrast to this, for the traveling mode, the magnitudes of u -component of the eigenvector at the shock and in the separated shear layer differ by only a factor of 5.

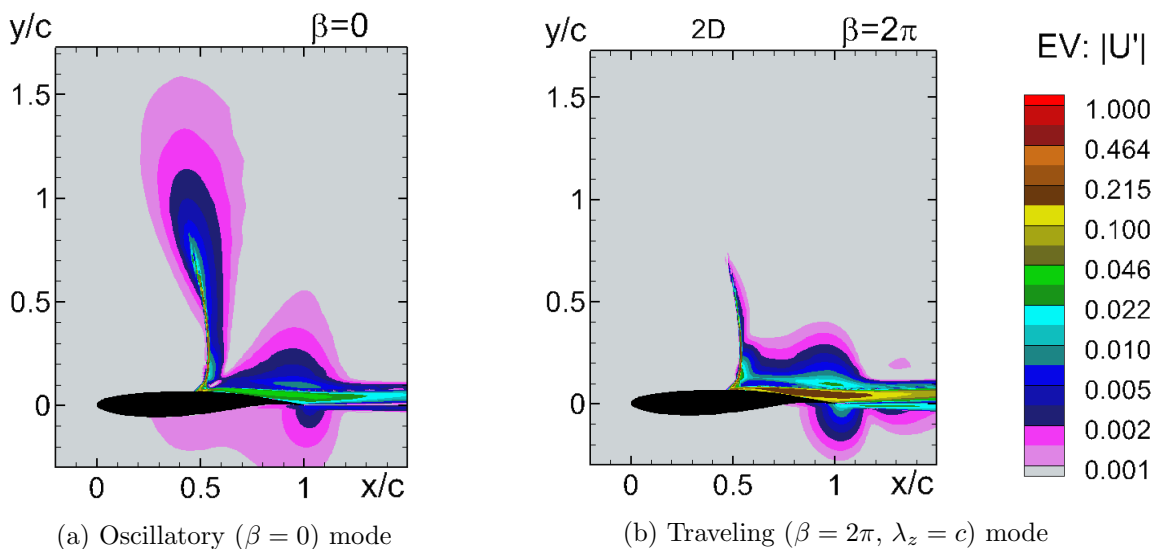


Figure 4. Contours of magnitude of u -component of eigenvectors of instability, normalized by the maximum, from q-3D stability analysis at $\alpha = 2.95^\circ$, $M_n = 0.73$

Figure 5 presents quantitative characteristics for the two unstable modes, showing the growth-rates and the frequencies of these modes as functions of the wavenumber β for the baseflow shown in Fig. 3 (negative values of β in this figure correspond to waves propagating in the direction opposite to the direction of the z axis, i.e. inboard).

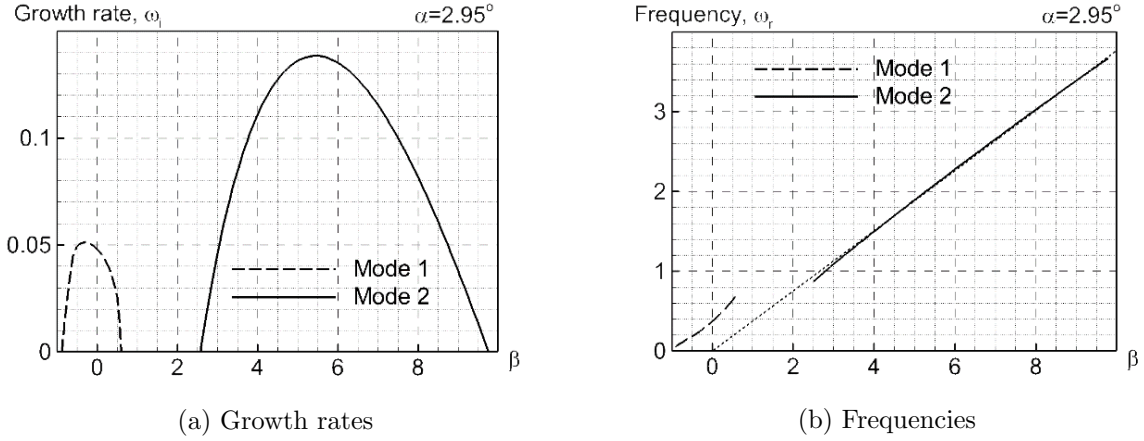


Figure 5. Characteristics of the oscillatory (Mode 1) and travelling (Mode 2) unstable modes as a function of wavenumber from q-3D stability analysis at $\alpha = 2.95^\circ$, $M_n = 0.73$

The Figure shows that the oscillatory mode (Mode 1 in the figure legend) is observed for $|\beta| < 1$, and is characterized by long-wavelength disturbances ($\lambda_z/c > 2\pi$). The frequency of these disturbances ω_r is less than ≈ 0.7 ($St = fc/U_n \approx 0.11$) and the maximum growth rate $\omega_{i,max}$ is equal to ≈ 0.05 . The maximum growth is reached in the vicinity of $\beta = 0$ (i.e., for the disturbances nearly uniform in the z -directions), and shows a slight bias towards inboard propagation.

The unstable traveling mode, which results in a spanwise undulating shape of the shock [9], is observed at wavenumbers β in the range from ≈ 2.5 up to ≈ 10 (λ_z/c from ≈ 0.63 up to ≈ 2.5). These wavelengths are intermediate to the long-wavelength oscillatory mode and shorter-wavelength traveling disturbances ($\lambda_z/c \approx 0.1$) observed for some flow conditions [2, 3]. The traveling mode frequency increases linearly with β and is significantly higher than that of the oscillatory mode. The maximum growth rate of the traveling mode occurs at $\beta \approx 5.5$ and is equal to ≈ 0.14 (almost 3 times larger than that of the oscillatory mode). For this reason, this mode has been observed to be dominate for both infinite [9] and finite [11, 23] swept wings. The following section focusses on this traveling mode to assess the different approaches used for the prediction of buffet onset.

3.2. Comparison of Approaches for Buffet Onset Prediction

The comparison of stability characteristics of the traveling mode predicted by q-3D analysis and fully-3D analysis at $\alpha = 2.95^\circ$ is presented in Fig. 6 and 7.

Figure 6 compares the predicted mode shapes in the form of the magnitude of the u -component of velocity at $\beta = 2\pi$. In the q-3D approach, this quantity is part of the 2D eigenfunction, and in the fully-3D analysis it is derived by spanwise-averaging of the 3D eigenfunction. Figure 7 presents the growth rate and frequency of the traveling mode as functions of β . The Figures show that the q-3D and fully-3D analyses return qualitatively-similar results for both the shape and the growth rate and frequency.

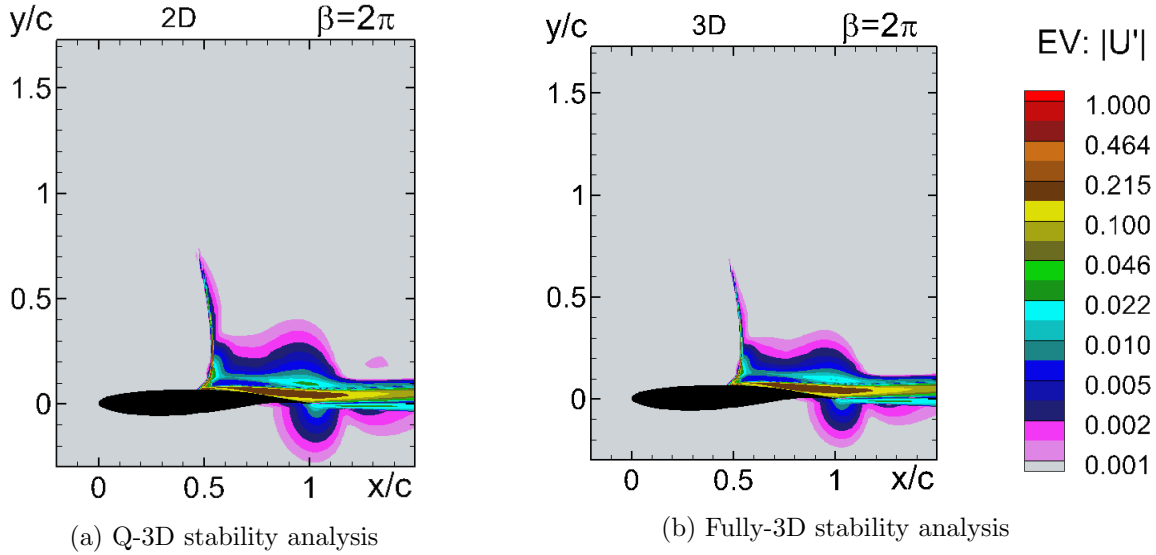


Figure 6. Contours of magnitude of u -component of traveling-mode eigenvectors normalized by the maximum at $\beta = 2\pi$ ($\lambda_z = c$) and $\alpha = 2.95^\circ$, $M_n = 0.73$

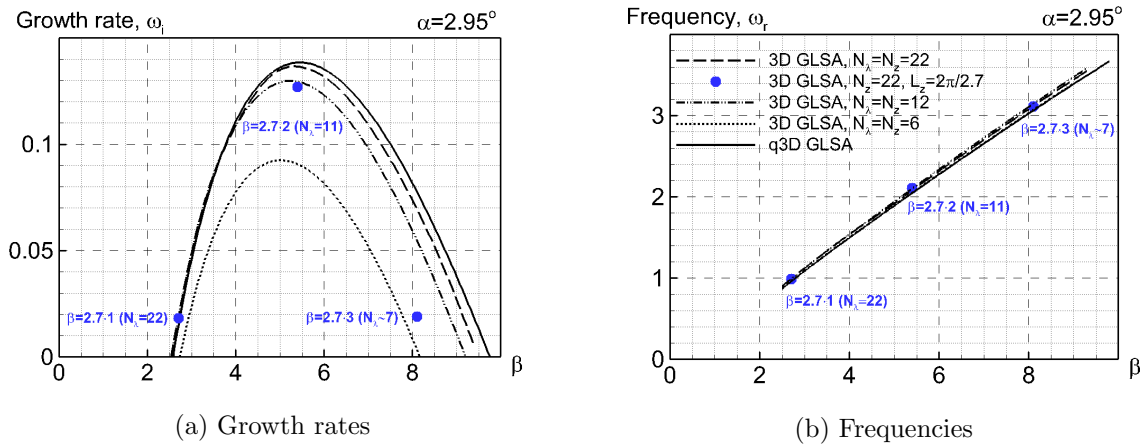


Figure 7. Comparison of characteristics for travelling mode of instability from q-3D and fully-3D stability analysis as functions of wavenumber at $\alpha = 2.95^\circ$, $M_n = 0.73$. GLSA stands for Global Linear Stability Analysis. Circles show the three least stable eigenvalues calculated at $\beta = 2.7$, $N_z = 22$

The growth rate for the fully-3D analysis is dependent on the number of grid planes in the z direction, but converges to the q-3D result with increasing grid resolution N_z . The fully-3D results (shown by the dashed lines) are based on $\beta = 2\pi/L_z$, so the N_z value is the number of grid planes per wavelength λ_z . As the value of N_z is increased from 6, to 12, and to 22, the fully-3D growth rates approach the q-3D curve. As noted earlier (and discussed in [8]), the fully-3D solution includes a set of discrete modes with $\lambda_z = L_z/m$, or $\beta = m \cdot 2\pi/L_z$. An example of these modes is shown by the blue symbols, for $\beta = m \cdot 2.7$, and $m = 1, 2, 3$. At the wavelength corresponding to $m = 1$, the N_z per wavelength is 22, and the growth rate falls on the curve associated with $N_z = 22$. For $m = 2$, the N_z per wavelength is 11, and the growth rate is just below the curve for $N_z = 12$. Likewise, for $m = 3$, the N_z per wavelength is approximately 7, and the growth rate is close to the $N_z = 6$ curve. These results show that the fully-3D growth rate is

very sensitive to the N_z per wavelength, so that unless the $m = 1$ mode is highly over-resolved, the higher modes ($m > 1$) need to be viewed with caution.

The frequencies shown in Fig. 7 have a much weaker sensitivity to the spanwise grid resolution. These frequencies are set by the spanwise propagation of the fixed-wavelength mode (along with the sweep angle [2, 14]), so they are not strongly dependent on finer details of the mode shape.

Finally, a direct comparison of the shapes of the 3D unstable traveling mode predicted by the q-3D and fully-3D stability analyses and by the 3D URANS simulations is provided in Fig. 8. This shows instantaneous fields of the normalized amplitude of the density component of this mode at $\beta = 2\pi$ ($\lambda_z/c = 1$) and $\alpha = 2.95^\circ$ on the wing upper surface computed with the use of these three approaches. This comparison shows very good agreement for the spatial structure of the unstable modes.

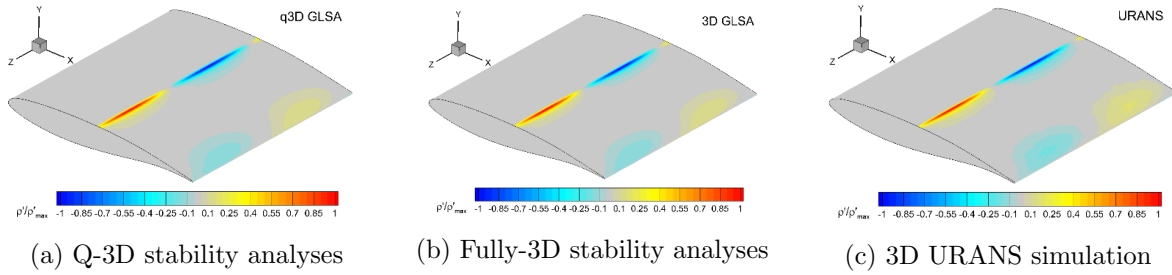


Figure 8. Comparison of normalized amplitude of density component of eigenvector on the airfoil surface at $\beta = 2\pi$ ($\lambda_z/c = 1$) and $\alpha = 2.95^\circ$, $M_n = 0.73$

We now consider the temporal variation of the 3D URANS solutions for the spanwise domain $L_z = 2c$ started from the steady 2.5D RANS solutions at supercritical values of the angle of attack. In general, after some transient period, the flow becomes unsteady with a periodic spatial variation in the spanwise direction with wavelength $\lambda_z/c = 1$ ($\beta = 2\pi$). This wavelength is close to the wavelength with the maximum growth rate for the traveling unstable mode, according to both the fully-3D and q-3D stability analysis (see Fig. 6a) and is admissible by the spanwise domain length $L_z = 2c$. At this stage of development, the amplitudes of the oscillations for all aerodynamic variables (i.e. their maximum deviation from the initial conditions) grow exponentially in time. This growth is illustrated in Fig. 9, showing the time-evolution of the v -component of the unsteady disturbance at the point $x = 1.05$, $y = 0$ for $\alpha = 2.95^\circ$, as an example. The growth rate ω_i deduced from these curves is equal ≈ 0.1 , which is roughly 0.03 below the stability results.

Similar post-processing of the 3D URANS solutions at other values of the angle of attack in the range 2.8° up to 3.0° , gives the dependence of $\omega_i(\alpha)$ shown in Fig. 10 together with the similar dependencies based on the q-3D and fully-3D stability analysis. The very small shift in the growth rate for the fully-3D stability analysis, compared to the q-3D result, is linked to the spanwise grid resolution as discussed for Fig. 7. The slightly lower growth rates for the URANS results are attributed to differences in the discretization errors compared to the stability formulations. Recall that the stability equations are derived and discretized independently, as opposed to using the discrete linearized operator from the URANS. The observation of generally-lower growth rates in the URANS for near-critical conditions has been observed in other applications as well [4, 5].

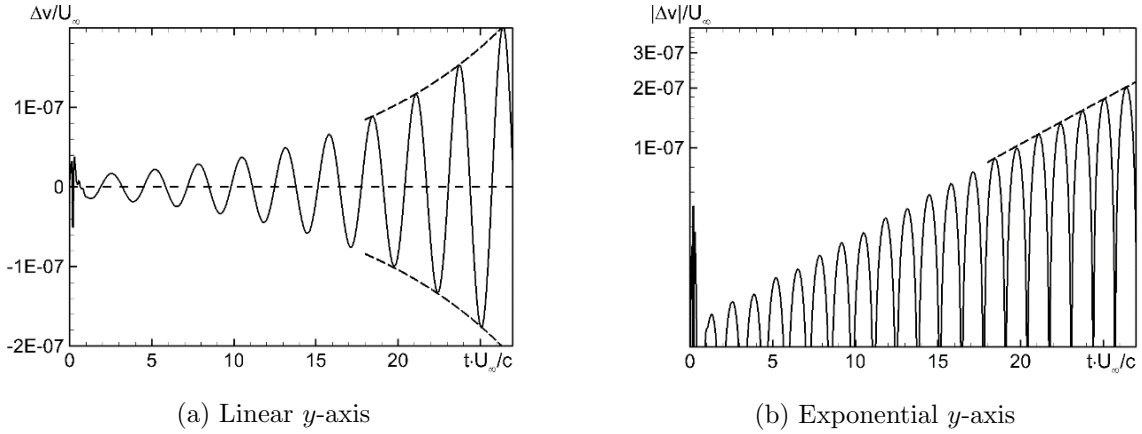


Figure 9. 3D URANS simulation results for the time-evolution of the v-velocity component of the disturbance in the linear stage of solution at $\alpha = 2.95^\circ$, $M_n = 0.73$. Dashed lines show amplitude of the disturbances as a function of time

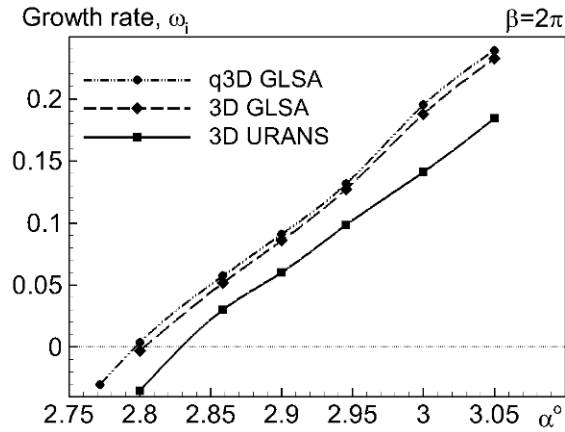


Figure 10. Comparison of growth rates for the travelling mode of instability at $\beta = 2\pi$ as a function of angle of attack, from q-3D and fully-3D stability analysis and 3D URANS simulations, $M_n = 0.73$

The small shifts in the growth rates translate to differences in critical conditions for the onset of buffeting as presented in Tab. 1. The value of α_{crit} is somewhat larger for the URANS simulations compared to the stability analysis. However, the difference of α_{crit} does not exceed 0.03 degrees (roughly 0.15% difference in lift at buffet onset). The maximum difference of the frequency of the disturbances predicted by the three approaches is about 2%. In practice, these overall differences are considered to be very small compared to other potential contributors (e.g. turbulence-model parameters).

Table 1. Critical angles of attack and corresponding frequencies for travelling mode at $\beta = 2\pi$ predicted by 3D URANS and the q-3D and fully-3D stability analysis for $M_n = 0.73$

Approach	α_{crit}	ω_r
3D URANS	2.83	2.36
3D stability	2.81	2.43
q-3D stability	2.80	2.37

Conclusion

A comparative study is performed for the three URANS-based approaches to predicting buffet onset and its characteristics for an infinite swept wing. Results are presented for the supercritical OAT15A airfoil, with that as an example. The most general of these approaches is based on the direct numerical solutions of 3D URANS equations, while two other approaches employ fully-3D and quasi-3D linear global stability analysis of the corresponding steady 2.5D RANS solutions. For this spanwise-uniform flow, q-3D stability analysis provides the most efficient and accurate representation of the instabilities leading to buffet onset. The fully-3D stability analysis, which does not require spanwise uniform flow, provides a potential link to more general wing configurations similar to the 3D URANS simulations.

Based on the analysis of the results of the 3D URANS and comparisons to the q-3D and fully-3D stability analysis, both stability formulations are shown to accurately capture the initial disturbance development. Spanwise-wavelength selection for the fully-3D analysis, as for the 3D URANS simulations, is dependent on the spanwise domain length. By varying the domain length, the fully-3D stability results are shown to capture the growth rates and frequencies predicted by the q-3D analysis. In addition, the spatial distributions of the disturbances over the wing cross-section plane are shown to be in good agreement for the different approaches. Stability predictions for the critical angle of attack for buffet onset at a given Mach number are in good agreement with the 3D URANS simulations (the difference is within the range of 0.03° , representing less than 0.15% in lift at buffet onset). The good overall agreement for these three independent formulations applied to the infinite swept wing provides a cross validation of the approaches.

Acknowledgements

The study is conducted with financial support of Russian Scientific Foundation, Grant No. 22-11-00041. The computations were performed on the HP computing facilities of the Peter the Great Saint-Petersburg Polytechnic University (<http://www.spbstu.ru>).

This paper is distributed under the terms of the Creative Commons Attribution-Non Commercial 3.0 License which permits non-commercial use, reproduction and distribution of the work without further permission provided the original work is properly cited.

References

1. Crouch, J.D., Garbaruk, A., Magidov, D., Travin, A.: Origin of transonic buffet on aerofoils. *Journal of Fluid Mechanics* 628, 357–369 (2009). <https://doi.org/10.1017/S0022112009006673>
2. Crouch, J.D., Garbaruk, A., Strelets, M.: Global instability in the onset of transonic-wing buffet. *Journal of Fluid Mechanics* 881, 3–22 (2019). <https://doi.org/10.1017/jfm.2019.748>
3. Crouch, J.D., Garbaruk, A., Strelets, M.: Global instability in the onset of transonic-wing buffet – CORRIGENDUM. *Journal of Fluid Mechanics* 901, E1 (2020). <https://doi.org/10.1017/jfm.2020.557>

4. Crouch, J., Garbaruk, A., Magidov, D.: Predicting the onset of flow unsteadiness based on global instability. *Journal of Computational Physics* 224(2), 924–940 (2007). <https://doi.org/10.1016/j.jcp.2006.10.035>
5. Garbaruk, A., Crouch, J.D.: Quasi-three dimensional analysis of global instabilities: onset of vortex shedding behind a wavy cylinder. *Journal of Fluid Mechanics* 677, 572–588 (2011). <https://doi.org/10.1017/jfm.2011.102>
6. Giannelis, N.F., Vio, G.A., Levinski, O.: A review of recent developments in the understanding of transonic shock buffet. *Progress in Aerospace Sciences* 92, 39–84 (2017). <https://doi.org/10.1016/j.paerosci.2017.05.004>
7. Gorobets, A.V., Duben, A.P.: Technology for supercomputer simulation of turbulent flows in the good new days of exascale computing. *Supercomputing Frontiers and Innovations* 8(4), 4–10 (Feb 2022). <https://doi.org/10.14529/jsfi210401>
8. He, W., Timme, S.: Triglobal infinite-wing shock-buffet study. *Journal of Fluid Mechanics* 925, A27 (2021). <https://doi.org/10.1017/jfm.2021.678>
9. Iovnovich, M., Raveh, D.E.: Numerical study of shock buffet on three-dimensional wings. *AIAA Journal* 53(2), 449–463 (2015). <https://doi.org/10.2514/1.J053201>
10. Jacquin, L., Molton, P., Deck, S., *et al.*: Experimental study of shock oscillation over a transonic supercritical profile. *AIAA Journal* 47(9), 1985–1994 (2009). <https://doi.org/10.2514/1.30190>
11. Koike, S., Ueno, M., Nakakita, K., Hashimoto, A.: Unsteady pressure measurement of transonic buffet on NASA common research model. In: 34th AIAA Applied Aerodynamics Conference, Washington, D.C., USA, June 13–17, 2016. <https://doi.org/10.2514/6.2016-4044>
12. Masini, L., Timme, S., Peace, A.J.: Analysis of a civil aircraft wing transonic shock buffet experiment. *Journal of Fluid Mechanics* 884, A1 (2020). <https://doi.org/10.1017/jfm.2019.906>
13. Paladini, E., Marquet, O., Sipp, D., *et al.*: Various approaches to determine active regions in an unstable global mode: application to transonic buffet. *Journal of Fluid Mechanics* 881, 617–647 (2019). <https://doi.org/10.1017/jfm.2019.761>
14. Paladini, E., Beneddine, S., Dandois, J., *et al.*: Transonic buffet instability: From two-dimensional airfoils to three-dimensional swept wings. *Phys. Rev. Fluids* 4, 103906 (Oct 2019). <https://doi.org/10.1103/PhysRevFluids.4.103906>
15. Plante, F., Dandois, J., Beneddine, S., *et al.*: Link between subsonic stall and transonic buffet on swept and unswept wings: from global stability analysis to nonlinear dynamics. *Journal of Fluid Mechanics* 908, A16 (2021). <https://doi.org/10.1017/jfm.2020.848>
16. Poplinger, L., Raveh, D.E., Dowell, E.H.: Modal analysis of transonic shock buffet on 2D airfoil. *AIAA Journal* 57(7), 2851–2866 (2019). <https://doi.org/10.2514/1.J057893>

17. Sartor, F., Timme, S.: Delayed detached-eddy simulation of shock buffet on half wing-body configuration. *AIAA Journal* 55(4), 1230–1240 (2015). <https://doi.org/10.2514/1.J055186>
18. Shur, M., Strelets, M., Travin, A.: High-order implicit multi-block Navier–Stokes code: Ten-year experience of application to RANS/DES/LES/DNS of turbulence. https://cfd.spbstu.ru/agarbaruk/doc/NTS_code.pdf (2008), accessed: 2009-10-01
19. Spalart, P., Allmaras, S.: A one-equation turbulence model for aerodynamic flows. In: 30th Aerospace Sciences Meeting and Exhibit, Reno, NV, USA, January 6–9, 1992. <https://doi.org/10.2514/6.1992-439>
20. Spalart, P.: Trends in turbulence treatments. In: Fluids 2000 Conference and Exhibit, Denver, CO, USA, June 19–22, 2000. <https://doi.org/10.2514/6.2000-2306>
21. Sugioka, Y., Koike, S., Nakakita, K., *et al.*: Experimental analysis of transonic buffet on a 3D swept wing using fast-response pressure-sensitive paint. *Experiments in Fluids* 59(6) (jun 2018). <https://doi.org/10.1007/s00348-018-2565-5>
22. Theofilis, V.: Global linear instability. *Annual Review of Fluid Mechanics* 43(1), 319–352 (2011). <https://doi.org/10.1146/annurev-fluid-122109-160705>
23. Timme, S.: Global instability of wing shock-buffet onset. *Journal of Fluid Mechanics* 885, A37 (2020). <https://doi.org/10.1017/jfm.2019.1001>